Journal of Biological Physics **26:** 85–112, 2000.

Parametric stabilization of biological coordination: a theoretical model

V.K. JIRSA, P. FINK, P. FOO and J.A.S. KELSO
Center for Complex Systems and Brain Sciences, Florida Atlantic University, Boca Raton, Florida 33431, U.S.A.
Corresponding author's email: jirsa@walt.ccs.fau.edu

Accepted in final form 15 February 2000

Abstract. In human coordination studies information from the environment may not only pace rhythmic behavior, but also contribute to the observed dynamics, e.g. a phenomenon known as anchoring in the literature. For the paradigmatic case of bimanual coordination we study these contributions mathematically and develop a model of the interaction between the limb's intrinsic dynamics and environmental signals from a metronome in terms of oscillator equations. We discuss additive versus multiplicative metronome impact and show the latter to be more appropriate. Our model describes single limb-metronome interaction, as well as multilimb-metronome interaction. We establish a parametric stabilization term which preserves the characteristics of bimanual coordination and additionally explains the varying stability of movement under different metronome conditions, the frequency dependence of the amplitudes of finger movements, anchoring phenomena and geometries of phase space trajectories. Predictions of our model are tested against experimental observations.

Key words: Auditory, coordination, dynamics, metronome, motor, parametric stabilization

1. Introduction

Experimental studies by one of us (Kelso, 1981; Kelso, 1984) have shown that abrupt phase transitions occur in self-paced human finger movements under the influence of scalar changes in cycling frequency. Phase transitions of a similar kind have also been found for coordination between different limbs (Byblow *et al.*, 1994; Kelso and Jeka, 1992), bimanual multifrequency coordination (DeGuzman and Kelso, 1991; Haken *et al.*, 1996; Kelso and DeGuzman, 1988) and coordination of swinging pendulums between subjects (Schmidt *et al.*, 1993; Amazeen *et al.*, 1995). However, in most of these experiments studying the coordination dynamics of human behavior a metronome is used commonly in order to scale the movement frequency of the subjects. That is, the metronome frequency acts as a non-specific control parameter that merely moves the system through different coordination states. Thus, as a first approximation it is usually assumed that the interaction with the metronome does not affect the coordination dynamics. As a result, most experimental and theoretical studies (see (Haken, 1996; Kelso, 1995)

for a review) do not account explicitly for any metronome driven effects vs. self-paced movement, even though the actual system under consideration is the human subject coordinating his/her behavior with the environment, i.e. the metronome (see (Kelso *et al.*, 1990; Schöner and Kelso, 1988a; Schöner and Kelso, 1988b; Tuller and Kelso, 1989; Zanone and Kelso, 1992) for environmentally specified coordination patterns). Here we want to show how specific information provided by the environment may qualitatively affect the global dynamics of rhythmic biological coordination patterns.

In the original self-paced bimanual coordination experiment by Kelso (Kelso, 1981; Kelso, 1984) the following phenomena were observed. Below a critical cycling frequency two dynamical patterns or coordination states are stable: An inphase state in which the finger movements are symmetric and an antiphase state in which finger movements are antisymmetric. Starting the finger movements in the antiphase state and increasing the cycling frequency, a spontaneous transition from antiphase to inphase occurs at the critical frequency. Beyond this frequency only the inphase state is stable. Further, it was experimentally observed that the amplitude of the finger movements decreases when the cycling frequency is increased, e.g. (Beek *et al.*, 1995; Kay *et al.*, 1987). In recent work (Fink *et al.*, 1998; Fink *et al.*, 1999) we investigated the paradigmatic case of inphase and antiphase bimanual finger coordination as the movement frequency was scaled from 1.4 to 3 Hz in 0.2 Hz steps every ten cycles under the impact of a metronome. Here we used two metronome conditions to control the movement frequency. In the single metronome condition participants were asked to move one complete cycle for each metronome beat such that the peak amplitude of right finger flexion was coincident with the metronome beat. In the double metronome condition participants were asked to move so that each finger reversal (flexion and extension) occurred simultaneously with the metronome beat. In the double metronome condition the metronome frequency was twice that of the single metronome condition so that the movement frequencies were identical for the two metronome conditions. The coordination dynamics of the double metronome condition was more stable than in the single metronome condition in the sense that transitions from antiphase occurred less frequently and always at a higher frequency. In those trials in which no transition occurred the standard deviation of the relative phase was lower in the double than in the single metronome condition. Differences in the amplitude behavior between the single and double metronome condition were also observed, with five of the six subjects exhibiting larger movement amplitudes in the double metronome condition. Additionally, previously unreported frequency-amplitude relations were observed, including increasing, decreasing, and an inverted u-shaped amplitude curve as frequency was increased. Another phenomenon, known as anchoring, was also observed in the data. Previous experiments (Byblow *et al.*, 1994; Carson, 1995; Carson *et al.*, 1994; Kelso *et al.*, 1991) have shown that movements are more temporally and spatially consistent at points in the movement linked with another event, i.e. a metronome. Anchoring can be seen in asymmetries in the $x - \dot{x} -$

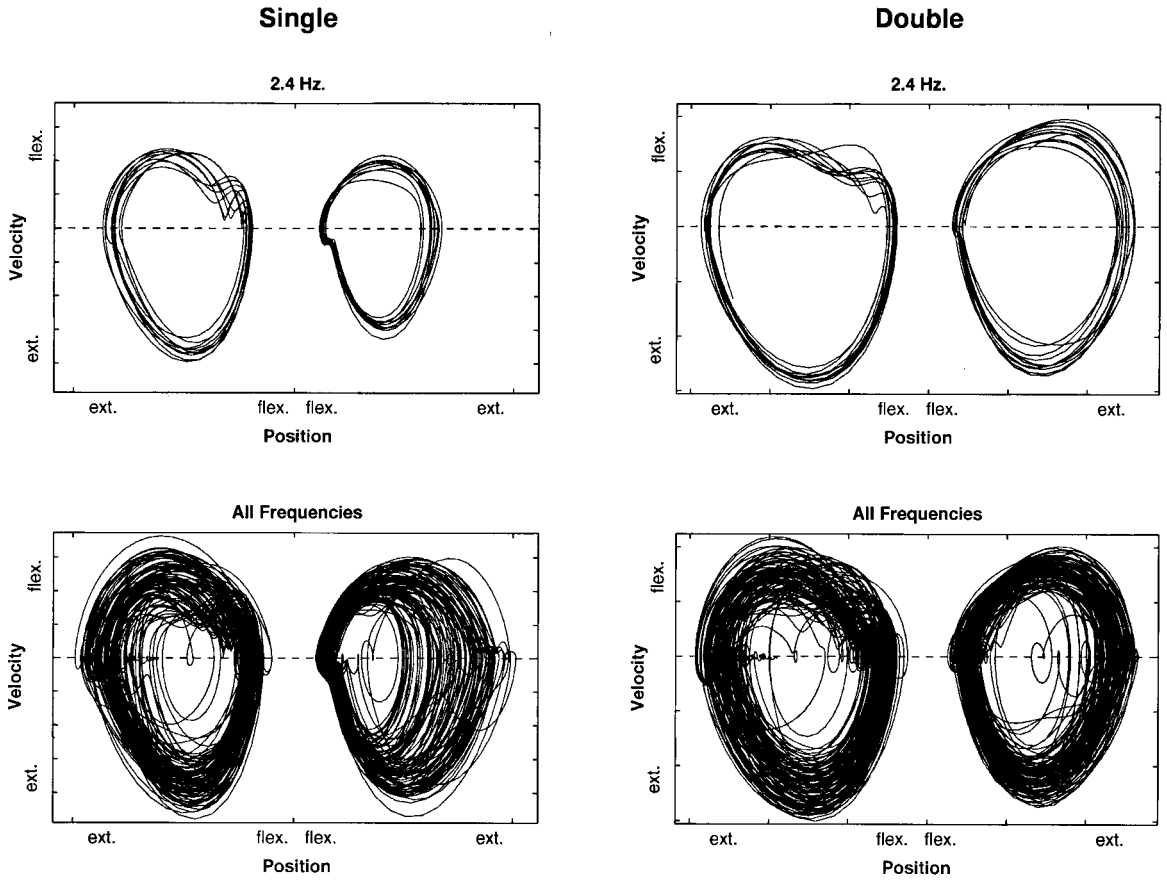

Figure 1. Phase plane trajectories of experimentally obtained left and right finger movements (in-phase) in $x - \dot{x}$ – space. Note that the x-axes of the left and right finger movements point in opposite directions. This is indicated by the location of the flexion and extension reversal points. Left: Trajectories for the single metronome condition with constant (top) and varying movement frequency (bottom). Right: Trajectories for the double metronome condition.

phase plane trajectories, with less variability at the reversal point coincident with the metronome beat than at the other reversal. In (Fink *et al.*, 1998) differences between anchored and unanchored reversals were also observed. The anchored reversal points generally displayed lower spatial variation than the unanchored reversal points within a frequency plateau and exhibited less of a shift in mean position as frequency was altered. The anchoring points are also spatially fixed in the phase space for the single metronome condition, even though movement frequency was varied and movement amplitude changed. This has not been observed for the double metronome condition. Together these effects resulted in phase plane trajectories for the entire trial that were thinner on one side than on the other in the single metronome condition (see Figure 1, left) and more symmetric in the double metronome condition (see Figure 1, right). The dashed horizontal line in Figure 1 denotes zero velocity. Thus, the intersections between the trajectories and the dashed line give the reversal points.

In the present study we investigate theoretically the metronome effect in the context of the previous models (Haken *et al.*, 1985; Schöner and Kelso, 1988a) and view these as limits for vanishing metronome impact. The main concept is that the metronome, under instructions to coincide one's action to it, acts as specific environmental information that serves to stabilize global coordination under conditions in which it would otherwise be susceptible to change, e.g. by switching to another coordination mode. This affords the biological system another means of adapting to a changing environment, i.e., stabilize rather than switch. We briefly review the original model (Haken *et al.*, 1985) for self-paced bimanual coordination in Section 2 as well as more recent neurally-based approaches (e.g. (Grossberg *et al.*, 1997; Nagashino and Kelso, 1992; Jirsa *et al.*, 1998)) in order to develop a formulation in Section 3 that incorporates additional interactions with external stimuli.

2. Bimanual coordination: self-paced

In 1985 the phenomena observed in bimanual coordination were theoretically modeled by Haken, Kelso and Bunz (HKB) (Haken *et al.*, 1985) in terms of the component variables x_1 and x_2, representing the amplitudes of the finger movements. The so-called HKB model reproduces the experimentally observed bistability, transition and hysteresis phenomena and reads

$$\ddot{x}_i + (Ax_i^2 + B\dot{x}_i^2 - \gamma)\dot{x}_i + \omega^2 x_i = f_i(x_1, x_2, \partial_t, 0) \text{ with } i = 1, 2 \tag{1}$$

where

$$f_1(x_1, x_2, \partial_t, 0) = (\dot{x}_1 - \dot{x}_2) \cdot (\alpha + \beta(x_1 - x_2)^2) \tag{2}$$

$$f_2(x_1, x_2, \partial_t, 0) = (\dot{x}_2 - \dot{x}_1) \cdot (\alpha + \beta(x_1 - x_2)^2) \tag{3}$$

The left hand side of (1) describes the motion of the individual fingers using a linear self-excitation, $\gamma > 0$, and Van-der-Pol and Rayleigh terms for saturation.

The right hand side describes the nonlinear coupling between the fingers by means of the coupling function $f_i(x_1, x_2, \partial_t, 0)$ dependent on x_1, x_2 and their temporal derivatives, indicated by the operator ∂_t. Here the zero in $f_i(x_1, x_2, \partial_t, 0)$ indicates the absence of the interaction with a metronome. These equations can be solved for small amplitudes by the following ansatz:

$$x_i = r_i e^{i\phi_i} e^{i\omega t} + r_i e^{-i\phi_i} e^{-i\omega t} \qquad \text{with} \qquad i = 1, 2 \tag{4}$$

where r_i is a real time dependent amplitude and ϕ_i a real time dependent phase. A mathematical analysis (Haken *et al.*, 1985) reveals the following properties of the model system:

- In the steady state the nontrivial amplitude of the oscillators is

$$r_i^2 = r^2 = \frac{\gamma}{A + 3B\omega^2} \tag{5}$$

  and depends on the cycling frequency ω. Here r_i is independent of the index i.
- The dynamics of the relative phase $\phi = \phi_1 - \phi_2$ can be derived from (1) and reads

$$\dot{\phi} = -a \sin\phi - 2b \sin 2\phi \tag{6}$$

  where

$$a = -(\alpha + 2\beta r^2) \qquad b = \frac{1}{2}\beta r^2 \; . \tag{7}$$

  Below the critical frequency ω_{c0} the relative phase ϕ is bistable with the two stable solutions $0, \pi$. Increasing the cycling frequency to ω_{c0} which is given by

$$r_c^2 = \frac{\gamma}{A + 3B\omega_{c0}^2} = \frac{-\alpha}{4\beta} \qquad \rightarrow \qquad \omega_{c0} = \sqrt{\frac{4\gamma\beta + \alpha A}{-3\alpha B}} \tag{8}$$

  the solution $\phi = \pi$ becomes unstable and the system (6) undergoes a transition to the remaining stable state $\phi = 0$.

The model system (1) reproduces the main experimental phenomena observed in the bimanual coordination experiment and predicts other properties, e.g. relaxation times, critical fluctuations and switching times that have been experimentally confirmed (Kelso *et al.*, 1986; Scholz *et al.*, 1987). More recently the dynamics in (1) has been derived directly from a biologically based neural theory (Jirsa *et al.*, 1998). On the basis of a neural ensemble theory (Jirsa and Haken, 1996; Jirsa and

Haken, 1997) a spatially extended continuous system describing cortical activity with sensorimotor and motor functional units was defined according to the bimanual coordination situation. The on-going brain activity was directly related to the behavioral coordination dynamics (Jirsa *et al.*, 1998) such that the parameters α, β and coupling terms in (1) could be expressed via neurophysiological quantities, e.g. the sigmoidal response curve of a neural ensemble. An experimental test by means of full-head magnetoencephalographic (MEG) recordings (Kelso *et al.*, 1994) provided preliminary confirmation of the theoretical predictions in (Jirsa *et al.*, 1998).

There are alternative more recent approaches which also find their motivation in biology. In (Grossberg *et al.*, 1997; Pribe *et al.*, 1997) a central pattern generator (CPG) model is used to explain the bimanual and multilimb coordination dynamics (see also (Nagashino and Kelso, 1992)). This approach is based on an expanded Elias-Grossberg oscillator (Elias and Grossberg, 1975) which uses shunting interactions between excitatory and inhibitory signals and on-center off-surround connectivity. Shunting processes are present in membrane equations (Hodgkin and Huxley, 1952) which is the neural basis of this system. The CPG model by (Grossberg *et al.*, 1997) requires periodic input signals which could be interpreted as metronome signals. The periodic input is introduced as linear and additive. In the present paper we will show that a linear additive input is not capable to produce phenomena like anchoring within the setting of an HKB model. This result does not directly apply to the CPG model by (Grossberg *et al.*, 1997), since it contains strong nonlinearities whereas the following analysis works in the weak nonlinearity limit. Here the mathematical advantage is the applicability of the tools from weakly nonlinear oscillator theory, e.g. (Guckenheimer and Holmes, 1983; Haken, 1983; Haken, 1987).

3. Bimanual coordination: paced

We consider a general coupling function $f_i(x_1, x_2, \partial_t, \epsilon(t))$ with $i = 1, 2$ dependent on the variables x_1, x_2 and a function $\epsilon(t)$. Here $\epsilon(t)$ describes some impact of an external stimulus on the system (1). In the simplest case which we will assume here, $\epsilon(t)$ may be identified with the external stimulus signal directly, however in reality $\epsilon(t)$ will usually represent a function or functional of the external stimulus signal. In case of an absent external stimulus we require that the original coupling functions of (1) are obtained

$$\lim_{|\epsilon(t)|\to 0} f_i(x_1, x_2, \partial_t, \epsilon(t)) = f_i(x_1, x_2, \partial_t, 0) \ . \tag{9}$$

The limit corresponds to a self-paced motion as described in Section 2. The HKB model operates in the weakly nonlinear regime. In the same spirit, we will con-

sider lower-order contributions of the stimulus signal, namely linear additive and multiplicative contributions:

$$f_i(x_1, x_2, \partial_t, \epsilon(t)) = f_i(x_1, x_2, \partial_t, 0) + \epsilon(t)(c_{0i} + \sum_{j=1}^{2} c_{ji} x_j + \sum_{j=1}^{2} d_{ji} \dot{x}_j + \text{h.o.t.}) \tag{10}$$

where h.o.t. denotes higher order terms. For small amplitudes (10) represents a Taylor expansion. Here we consider additive and multiplicative linear couplings only. Because of the requirement (9) there are no other terms solely in x_1, x_2 and their derivatives, except the ones contained in $f_i(x_1, x_2, \partial_t, 0)$, and the stimulus $\epsilon(t)$ is multiplicative only in (10). Higher orders of the stimulus $\epsilon(t)$ are not considered here. The constant coefficients are given by c_{0i}, c_{ji}, d_{ji} where $j = 1, 2$ and $i = 1, 2$. Further, we postulate $c_{12}, c_{21}, d_{12}, d_{21} \approx 0$, since these coefficients represent simultaneous cross-coupling between both fingers and the metronome signal, i.e. we assume that the metronome signal drives each finger independently. This can be motivated by the fact that similar transition and bistability phenomena are observed in the rhythmic coordination of one finger and an external metronome (Kelso *et al.*, 1990). We will return to this issue later in the analytical discussion of (10). From the mere presence of an independent coupling between one finger and the metronome signal we cannot infer the validity of this independent coupling for the bimanual case, but it serves as a starting point in our study. Finally, we do not consider any symmetry breaking, e.g. due to handedness or laterality (but see e.g. (Treffner and Turvey, 1996)). Both fingers are assumed to be equivalent resulting in the invariance of Equation (1) under the exchange of the variables $x_1 \rightarrow x_2$ and $x_2 \rightarrow x_1$ and also their derivatives. This invariance condition restricts the coefficients to

$$c_{01} = c_{02} = c_0 \qquad c_{11} = c_{22} = c_1 \qquad c_{12} = c_{21} \approx 0 \tag{11}$$

and

$$d_{11} = d_{22} = d_1 \qquad d_{12} = d_{21} \approx 0 \tag{12}$$

Our resulting coupling function reads

$$f_i(x_1, x_2, \partial_t, \epsilon(t)) = f_i(x_1, x_2, \partial_t, 0) + c_0\epsilon(t) + c_1 x_i \epsilon(t) + d_1 \dot{x}_i \epsilon(t) + \text{h.o.t.} \tag{13}$$

which contains the original HKB coupling to third order and an additional coupling to the external stimulus $\epsilon(t)$ signal containing terms of x_i, $\dot{x}_i$ with $i = 1, 2$.

3.1. PERIODIC METRONOME SIGNAL

In the experiment periodic finger movements are performed where the time period T is given by the metronome such that $\epsilon(t) = \epsilon(t+T)$. Here we operationalize the T-periodic metronome signal by a sinusoid*

$$\epsilon(t) = \epsilon_0 \cos \Omega t \qquad \text{where} \qquad \Omega = \frac{2\pi}{T} \tag{14}$$

We truncate the coupling function after the first order and obtain after inserting (14)

$$\begin{aligned} f_i(x_1, x_2, \partial_t, \epsilon(t)) = f_i(x_1, x_2, \partial_t, 0) + c_0\epsilon_0 \cos \Omega t + c_1\epsilon_0 \cos \Omega t \; x_i \\ + d_1\epsilon_0 \cos \Omega t \; \dot{x}_i \end{aligned} \tag{15}$$

where the first driving term is a linear driving, the second and third term a parametric excitation. Note that a linear driving has been suggested earlier as an intentional and environmentally-specified effect (Schöner and Kelso, 1988a; Schöner and Kelso, 1988b).

In the following we perform an analytic discussion of the equation

$$\ddot{x}_i + (Ax_i^2 + B\dot{x}_i^2 - \gamma)\dot{x}_i + \omega^2 x_i = f_i(x_1, x_2, \partial_t, \epsilon(t)) \;\text{ with }\; i = 1, 2 \tag{16}$$

where the rhs is given by (15). We will show that the linear driving term $\epsilon_0 \cos \Omega t$ cannot account for most of the experimentally phenomena, but rather that the parametric driving is the relevant contribution. The latter has the characteristic property of having stable and unstable solutions dependent on the ratio of ω and Ω. The unstable solutions are obtained for

$$\frac{\omega}{\Omega} = k \;, \qquad \text{where} \qquad k = 1/2,\; 1,\; 3/2, \ldots \tag{17}$$

A stability diagram is given in Figure 2 showing the instability and stability regimes in the parameter space $\Omega - \epsilon$. The light regions are called Arnold tongues and denote unstable regimes. Note that instability regime denotes the region where the oscillatory state of zero activity becomes unstable and an oscillatory state of non-zero activity and frequency ratio $k = \omega/\Omega$ is occupied. The instability regime describes a region of stable $1 : k$ coordination for which k increases from right to left in Figure 2. Outside of the Arnold tongues drifting solutions are obtained, i.e. there is no phase and frequency locking. Since we are concerned with two types of coordination, 1:1 and 1:2, the two Arnold tongues on the right of Figure 2 are of interest. Note how much wider the right Arnold tongue for 1:2 coordination is than all the others. In the following we consider two cases: 1. In the double metronome case the metronome frequency Ω is about twice the eigenfrequency ω of the oscillators x_1, x_2, i.e. the stimulus signal is presented at full extension and full flexion. We

* Note that parametric stabilization also occurrs for periodic rectangular stimuli.

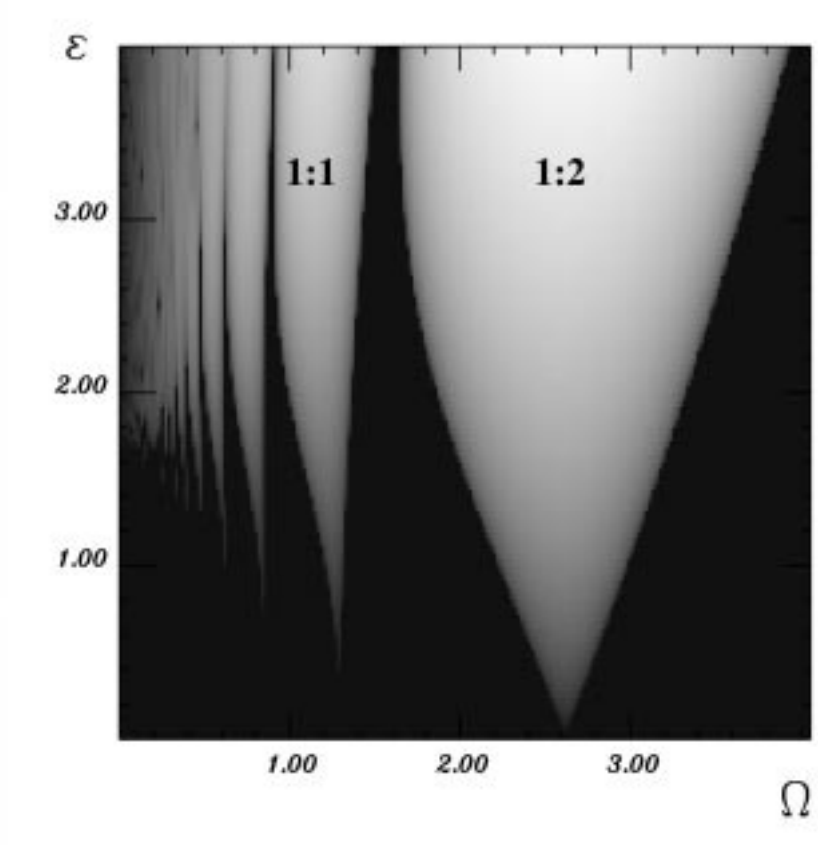

Figure 2. Instability regions of parametrically excited oscillators. The amount of instability is coded for increasing values from black to white. The instability regions are plotted in dependence of varying coupling strength ϵ and metronome frequency Ω. Unstable solutions are obtained for $\omega/\Omega = k$, where $k = 1/2, 1, 3/2, \ldots$ and increases from right to left, i.e the largest instability regime is on the right corresponding to $\omega : \Omega = 1 : 2$. A movement along a horizontal line for a fixed parameter value ϵ_0 corresponds to a scaling of the metronome frequency and leads through both coordination regimes (double metronome 1:2 and single metronome 1:1).

interpret this situation such that the oscillators x_1, x_2 operate in the first instability regime with $k = 1/2$. 2. In the single metronome case the metronome frequency Ω is in the same range as the eigenfrequency ω corresponding to operation within the second instability regime with $k = 1$. We distinguish two regimes of coupling strength ϵ_0:

– For small coupling strength ϵ_0 the dynamics of (16) is determined by the limit $\epsilon_0 \to 0$ where no interaction with the metronome is considered and is discussed in Section 2.

– For strong coupling strength ϵ_0 the dynamics of (16) changes qualitatively. We refer to this situation as *parametric stabilization* and specify its properties in more detail. We will treat (16) analytically and numerically in the following sections and elaborate the main difference between self-paced and triggered environmentally specified coordination.

3.2. THE DOUBLE METRONOME CASE

Our starting point is Equation (16) and the assumption $\omega \approx \Omega/2$, i.e. the eigenfrequency ω corresponds to the movement frequency (as in the HKB model (Haken *et al.*, 1985)) and changes as the metronome frequency Ω varies. We choose the following ansatz for the solutions:

$$x_j(t) = x_{j+}e^{i\Omega/2t} + x_{j-}e^{-i\Omega/2t} \tag{18}$$

where x_{j+}, x_{j-} denote time dependent complex coefficients. We insert (18) into (16) and perform two approximations, the slowly varying amplitude approximation and the rotating wave approximation (see (Haken, 1983; Haken, 1987) for details). The first accounts for the fact that x_{j+}, x_{j-} act on a time scale which is much smaller than that given by the metronome signal; the latter neglects higher frequency contributions. We split the complex variables x_{j+}, x_{j-} into its real amplitude $r_j \in \Re$ and real phase $0 \leq \phi_j < \pi$ as follows

$$x_{j+} = r_j e^{i\phi_j} \qquad x_{j-} = r_j e^{-i\phi_j} \tag{19}$$

Note that here we do not use the typical transformation into polar coordinates, but rather also allow for negative amplitudes r_j. With these operations and the abbreviation $\phi = \phi_1 - \phi_2$ we can reduce (16) to a set of amplitude equations

$$\begin{aligned} \dot{r}_1 \;=\; & \tfrac{\gamma+\alpha}{2}\, r_1 - \tfrac{\alpha}{2}\, r_2 \,\cos\phi + \tfrac{1}{2}\beta(r_1^2 + r_2^2 - 2r_1 r_2 \cos\phi)\cdot(r_1 - r_2\cos\phi) \\ & -\tfrac{1}{2}(A + \tfrac{3}{4}B\Omega^2)\, r_1^3 + c_1\tfrac{\epsilon_0}{2\Omega}\sin 2\phi_1\, r_1 + d_1\tfrac{\epsilon_0}{4}\cos 2\phi_1\, r_1 \end{aligned} \tag{20}$$

$$\begin{aligned} \dot{r}_2 \;=\; & \tfrac{\gamma+\alpha}{2}\, r_2 - \tfrac{\alpha}{2}\, r_1 \,\cos\phi + \tfrac{1}{2}\beta(r_1^2 + r_2^2 - 2r_1 r_2 \cos\phi)\cdot(r_2 - r_1\cos\phi) \\ & -\tfrac{1}{2}(A + \tfrac{3}{4}B\Omega^2)\, r_2^3 + c_1\tfrac{\epsilon_0}{2\Omega}\sin 2\phi_2\, r_2 + d_1\tfrac{\epsilon_0}{4}\cos 2\phi_2\, r_2 \end{aligned} \tag{21}$$

and a set of phase equations

$$\begin{aligned} \dot{\phi}_1 = {} & \frac{4\omega^2 - \Omega^2}{4\Omega} + \frac{1}{2}(\alpha + \beta(r_1^2 + r_2^2))\frac{r_2}{r_1}\sin\phi - \frac{1}{2}\beta r_2^2 \sin 2\phi \\ & + c_1\frac{\epsilon_0}{2\Omega}\cos 2\phi_1 + d_1\frac{\epsilon_0}{4}\sin 2\phi_1 \end{aligned} \tag{22}$$

$$\dot{\phi}_2 = \frac{4\omega^2 - \Omega^2}{4\Omega} - \frac{1}{2}(\alpha + \beta(r_1^2 + r_2^2))\frac{r_1}{r_2}\sin\phi + \frac{1}{2}\beta r_1^2 \sin 2\phi \\ + c_1\frac{\epsilon_0}{2\Omega}\cos 2\phi_2 + d_1\frac{\epsilon_0}{4}\sin 2\phi_1 \tag{23}$$

There is no contribution of the linear driving with c_0 to the oscillator Equations (20)–(23) in the double metronome case, thus here the linear driving does not qualify as a candidate coupling between rhythmic finger movements and external metronome. The parametric driving contributions with c_1, d_1 have qualitatively the same impact distinguished by a phase shift $\pi/4$ and a factor $\Omega/2$. At present quantitative statements about the coupling terms cannot be made, however, we can focus on the nature of it and discuss its qualitative properties, thus we set $c_1 = 1$, $d_1 = 0$ here and in the following. Subtracting (23) from (22) we receive the following equation for the dynamics of the relative phase ϕ

$$\dot{\phi} = \frac{1}{2}(\alpha + \beta(r_1^2 + r_2^2))\,(\frac{r_2}{r_1} + \frac{r_1}{r_2})\sin\phi - \frac{1}{2}\beta(r_1^2 + r_2^2)\sin 2\phi \\ + \frac{\epsilon_0}{2\Omega}(\cos 2\phi_1 - \cos 2\phi_2) \tag{24}$$

The oscillator system (16) shall be well stabilized by the parametric driving, meaning that the stationary states of the phases ϕ_1 and ϕ_2 are mainly determined by the parametric driving corresponding to a strong coupling ϵ_0. A fundamental property of a parametrically driven system is that once the phases are locked, the corresponding amplitudes r_1, r_2 may become unstable, i.e. the oscillators operate in the instability regimes as shown in Figure 2. The maximum amplitudes are obtained when $\sin 2\phi_i$ with $i = 1, 2$ in (20), (21) becomes maximal, i.e. the system roughly operates in the middle of the instability regimes. This situation is given when (22), (23) can be approximated by

$$\dot{\phi}_1 \approx \frac{\epsilon_0}{2\Omega}\cos 2\phi_1 = 0 \tag{25}$$

$$\dot{\phi}_2 \approx \frac{\epsilon_0}{2\Omega}\cos 2\phi_2 = 0 \tag{26}$$

leading to the stable stationary values $\phi_1 = \pi/4$ modulo π and $\phi_2 = \pi/4$ modulo π for big enough ϵ_0. This condition of parametric stabilization equals an adiabatic elimination of the phases ϕ_1, ϕ_2. We rewrite the phase $\phi_1 = \phi_2 + \phi$ and insert this into (24), so we can express the dynamics of the relative phase as follows

$$\dot{\phi} = -a\sin\phi - 2b\sin 2\phi \tag{27}$$

with

$$a = -\frac{1}{2}(\alpha + \beta(r_1^2 + r_2^2))\,(\frac{r_2}{r_1} + \frac{r_1}{r_2}) \qquad b = \frac{1}{2}(\frac{\epsilon_0}{\Omega} + \beta(r_1^2 + r_2^2)) \tag{28}$$

Table I. Parameters used in the simulations for self-paced (HKB) and paced (single and double metronome condition) movement

HKB	Single	Double
$A = B = 1, \alpha = -0.2, \beta = 0.2$		
$\gamma = 1, \epsilon = 0$	$\gamma = 0.01, \epsilon = 3$	
$\omega = \Omega$		$\omega = \frac{1}{2}\Omega$

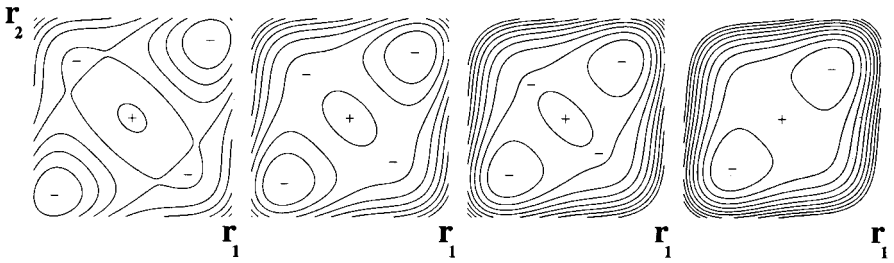

Figure 3. Potential landscape in the double metronome case. Isoclines of the potential V in dependence of movement amplitudes r_1, r_2 are plotted for increasing values of the control parameter Ω from left to right.

Equations (27) and (28) represent the classic formulation of the phase dynamics HKB. In the following we simplify the system and move to an amplitude picture.

Under parametric stabilization these coefficients are well approximated by $a \approx 0$ and $b \approx \epsilon_0/2\Omega$ which reduces (27) to

$$\dot{\phi} \approx -\frac{\epsilon_0}{2\Omega} \sin 2\phi \tag{29}$$

The relative phase ϕ has the stable stationary solution $\phi = 0$ modulo π. The approximations (25),(26) and (29) are tested numerically and prove to be very good for the stationary states. The actual transition dynamics under these approximations will be discussed in the following. The limitations of these approximations are studied in Section 4.3. The amplitude Equations (20) and (21) can be expressed by a potential dynamics:

$$\dot{r}_1 = -\frac{\partial V}{\partial r_1} \qquad \text{and} \qquad \dot{r}_2 = -\frac{\partial V}{\partial r_2} \tag{30}$$

where the potential V is given by

$$\begin{aligned} V &= -\tfrac{1}{4}(\gamma+\alpha)\cdot(r_1^2+r_2^2) - \tfrac{\epsilon_0}{4\Omega}(\sin 2\phi_1 r_1^2 + \sin 2\phi_2 r_2^2) \\ &\quad + \tfrac{\alpha}{2}\cos\phi r_1 r_2 + \tfrac{1}{8}(A+\tfrac{3}{4}B\Omega^2)(r_1^4+r_2^4) \\ &\quad - \tfrac{1}{2}\beta(\tfrac{1}{4}(r_1^2+r_2^2)^2 - r_1 r_2\cos\phi(r_1^2+r_2^2+r_1 r_2\cos\phi)) \end{aligned} \tag{31}$$

In Appendix A we calculate the stationary solutions of (30) and perform a linear stability analysis. Below a critical frequency ω_{c2} there are stable stationary solutions

$$r_1 = r_2 = \sqrt{\frac{\epsilon_0+\Omega\gamma}{\Omega(A+\frac{3}{4}B\Omega^2)}} \tag{32}$$

describing the inphase situation and

$$r_1 = -r_2 = \sqrt{\frac{\epsilon_0+\Omega(\gamma+2\alpha)}{\Omega(A+\frac{3}{4}B\Omega^2)}} \tag{33}$$

describing the antiphase situation. Here ω_{c2} denotes the critical finger movement frequency corresponding to half the critical metronome frequency. Above the critical frequency the antiphase solutions become unstable. The critical frequency is given by

$$\omega_{c2} = \frac{-\epsilon_0}{2(3\alpha+\gamma)} \tag{34}$$

The dependence of the potential V is plotted in Figure 3 for increasing values of the control parameter Ω from 4 to 5.5 which corresponds to a movement frequency ω of 2 to 2.75. The minus sign denotes a local minimum, the plus sign a local maximum in the potential landscape. The parameters used in the numerical simulations are given in Table I, Section 4.1. Here it can be seen that two possible states, antiphase and inphase are existent, below a critical value of the control parameter. At this critical value the antiphase state becomes unstable and a transition occurs into the inphase state. This transition occurs such that the amplitude of one of the oscillators breaks down in the antiphase state, crosses the coordinate axis and comes up again in the inphase state. Within the potential landscape of Figure 3 this behavior corrresponds to a motion of one of the oscillators from the antiphase minimum to the inphase minimum by crossing the coordinate axis.

Traditionally, transitions in coordination behavior are described in polar coordinates by the relative phase between the components (e.g. (Kelso, 1984)). Thus a transition from antiphase to inphase is described by positive amplitudes r_1, r_2 and the change of the relative phase ϕ from π to 0. An equivalent description of this transition is in terms of constant relative phase ϕ and a transition of one of the

amplitudes to its negative value, e.g. $r_1 \rightarrow -r_1$, as employed here. This description differs from the prior in terms of its amplitude dynamics, namely the simultaneous change of the amplitude during the transition.

3.3. THE SINGLE METRONOME CASE

The frequency relation of the single metronome case reads $\omega \approx \Omega$. We choose the following ansatz for the solutions:

$$x_j(t) = x_{j0} + x_{j+}e^{i\Omega t} + x_{j-}e^{-i\Omega t} \tag{35}$$

with x_{j0} denoting a time dependent real coefficient and x_{j+}, x_{j-} denoting time dependent complex coefficients. The latter are split again into their amplitude and phase contributions according to (19). In the single metronome case the oscillator system shall operate within the second instability regime (see Figure 2). Here we use the ansatz (35), since the term x_{j0} describing a shift of the zero points of the oscillators contributes to the dynamics. This term can be adiabatically eliminated (see (Haken, 1983; Haken, 1987)), i.e. $\dot{x}_{j0} \approx 0$, and its dynamics is expressed as a function of x_{j+}, x_{j-}:

$$x_{j0} = -\frac{\epsilon_0}{2\omega^2}(x_{j+} + x_{j-}) \tag{36}$$

The same steps as in the double metronome case may now be performed: Under parametric stabilization the dynamics of the phases ϕ_1, ϕ_2 can be expressed by

$$\dot{\phi}_1 \approx -\frac{\epsilon_0^2}{8\Omega\omega^2}\cos 2\phi_1 = 0 \tag{37}$$

$$\dot{\phi}_2 \approx -\frac{\epsilon_0^2}{8\Omega\omega^2}\cos 2\phi_2 = 0 \tag{38}$$

leading to the stable stationary values $\phi_1 = -\pi/4$ modulo π and $\phi_2 = -\pi/4$ modulo π. The relative phase equation reduces to

$$\dot{\phi} \approx -\frac{\epsilon_0^2}{8\Omega\omega^2}\sin 2\phi \tag{39}$$

in analogy to (29).

Then we obtain the following dynamics of the amplitudes

$$\begin{aligned}\dot{r}_1 = {} & \frac{\gamma+\alpha}{2}\, r_1 - \frac{\alpha}{2}\, r_2 \cos\phi - \frac{1}{2}(A(\frac{\epsilon_0^2}{2\omega^4}(\cos 2\phi_1 + 1) + 1) \\ & + 3B\Omega^2)\, r_1^3 - \frac{\epsilon_0^2}{8\Omega\omega^2}\sin 2\phi_1\, r_1 - \frac{c_0\epsilon_0}{2\Omega}\sin\phi_1\end{aligned} \tag{40}$$

$$\dot{r}_2 = \frac{\gamma+\alpha}{2}\, r_2 - \frac{\alpha}{2}\, r_1 \cos\phi - \frac{1}{2}(A(\frac{\epsilon_0^2}{2\omega^4}(\cos 2\phi_1 + 1) + 1) + 3B\Omega^2)\; r_2^3 - \frac{\epsilon_0^2}{8\Omega\omega^2}\sin 2\phi_2\, r_2 - \frac{c_0\epsilon_0}{2\Omega}\sin\phi_2 \tag{41}$$

where we dropped the terms with the coefficient β for brevity since they change the dynamics only quantitatively. The full phase and amplitude equations are given in Appendix B. The last two terms in (40), (41) describe the interaction with the external metronome signal where the first determines the impact of parametric driving and the second the impact of linear driving. The parametric driving term turns out to be π-periodic which means bistability is preserved and any stabilization via this driving acts on both stationary states of the relative phase, i.e. inphase and antiphase. The linear driving term is 2π-periodic which enforces monostability and stabilization of only one stationary state of the relative phase, whereas the other state is destabilized. Hence the parametric driving qualifies as the best candidate for the external stabilizing force. Since the linear driving destroys the bistability of the oscillator system, we postulate the constraint $c_0 \ll c_1$.

The stationary solutions of the amplitudes r_1, r_2 and their stability are calculated in Appendix A. Below the critical frequency

$$\omega_{c1} = (\frac{-\epsilon_0^2}{4(3\alpha+\gamma)})^{1/3} \tag{42}$$

the stable stationary solutions are

$$r_1 = r_2 = \sqrt{\frac{\epsilon_0^2 + 4\omega^2\Omega\gamma}{4\omega^2\Omega(A(1+\epsilon_0^2/(2\omega^4)) + 3B\Omega^2)}} \tag{43}$$

for inphase and

$$r_1 = -r_2 = \sqrt{\frac{\epsilon_0^2 + 4\omega^2\Omega(\gamma+2\alpha)}{4\omega^2\Omega(A(1+\epsilon_0^2/(2\omega^4)) + 3B\Omega^2)}} \tag{44}$$

for antiphase. Above the critical frequency the antiphase solutions become unstable.

The amplitude Equations (40) and (41) can also be expressed by a potential dynamics:

$$\dot{r}_1 = -\frac{\partial V}{\partial r_1} \qquad \text{and} \qquad \dot{r}_2 = -\frac{\partial V}{\partial r_2} \tag{45}$$

where the potential V is given by

$$\begin{aligned} V \;=\; & -\tfrac{1}{4}(\gamma+\alpha)\cdot(r_1^2+r_2^2) + \tfrac{\epsilon_0^2}{16\Omega\omega^2}(\sin 2\phi_1 r_1^2 \\ & + \sin 2\phi_2 r_2^2) + \tfrac{\alpha}{2}\cos\phi r_1 r_2 + \tfrac{1}{8}(A+3B\Omega^2)(r_1^4+r_2^4) \\ & + A\tfrac{\epsilon_0^2}{16\omega^4}((\cos 2\phi_1+1)r_1^4 + (\cos 2\phi_2+1)r_2^4) \end{aligned} \tag{46}$$

A plot of the potential dynamics is analogeous to the one in Figure 3.

4. Numerical results

4.1. AMPLITUDE DYNAMICS AND TRANSITION PHENOMENA

In the HKB model (Haken *et al.*, 1985) the analytically obtained stationary amplitudes of r_1, r_2 were determined under the approximation that the coupling terms in α, β in (2), (3) do not contribute to the amplitude dependence. This approximation is sufficient if only the transition behavior of the relative phase ϕ is examined. It is not sufficient if also the difference in the amplitudes before and after the transition are to be investigated. A more detailed examination (Kay *et al.*, 1987) of the amplitudes of r_1, r_2 which also takes the coupling terms in (2), (3) into account, reveals their stationary values

$$r_i^2 = r^2 = \frac{\gamma + \alpha(1 - \cos\phi)}{A + 3B\Omega^2 - 2\beta(1 - \cos\phi)^2} \tag{47}$$

with $i = 1, 2$. Equation (47) shows that the stationary amplitudes also depend on the relative phase ϕ, but both amplitudes r_1, r_2 are equal.

In the single and in the double metronome case the approximation $r_1 = r_2 = r$ is not appropriate. We included the coupling terms α, β in the analytic discussion of the amplitudes in the preceding Sections 3.2 and 3.3. For the analytic calculation of the stationary amplitudes and critical transition frequencies we neglected the β terms, since their contributions are small in the case of parametric stabilization. A comparison of the analytically determined stationary amplitudes shows that the amplitudes in the double metronome case (Equations (32), (33)) are significantly larger than in the single metronome case (Equations (43), (44)). For the parameter range $2.4 < \epsilon_0 < 3.1$ (see Section 4.2) the amplitude in the double metronome case is 20% to 90% larger than the amplitude in the single metronome case. In the experiment (Fink *et al.*, 1999), ratios of 10% to 60% were observed for different subjects and conditions.

In Figure 4 we compare our analytical results with numerical simulations for the three cases HKB, single and double metronome. On the lhs the transitional behavior of the oscillators x_1, x_2 is plotted over the time t at the corresponding critical frequency. The qualitative difference between self-paced and paced movement can be clearly seen: In the former case a shift in the relative phase occurs, in the latter one of the oscillators collapses to zero and regenerates with opposite sign of amplitude, but constant relative phase. Both types of behavior have been observed in single runs of experimental data (Fink *et al.*, 1999). The constant relative phase during the amplitude transition is consistent with our approximation (29), (39) of the relative phase dynamics. We checked the validity and limitations of this approximation by direct numerical simulations of the amplitude and phase equations (double: (20)-(23), single: (63)-(66)) in Section 4.3.

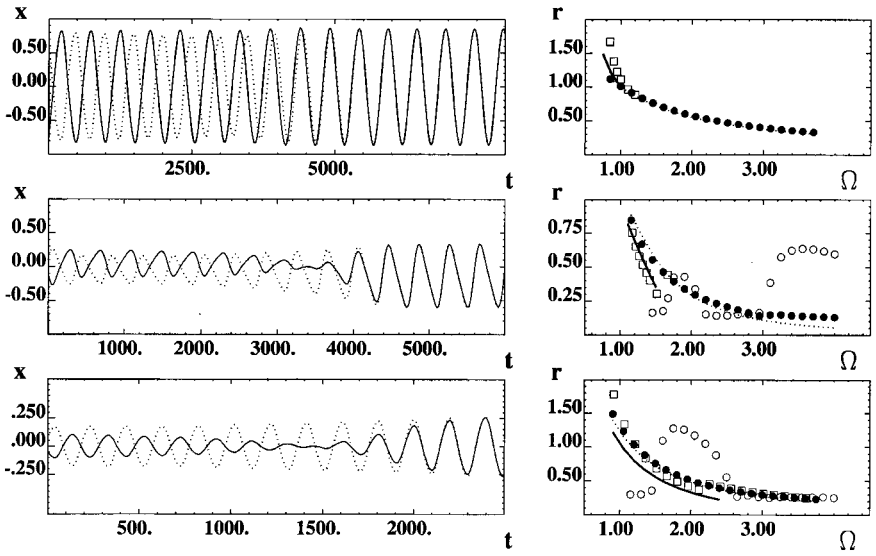

Figure 4. Transition dynamics and amplitude dependence. The time series of the finger movements x_1, x_2 are plotted during the transition (left column). Three cases are distinguished: HKB (top), single metronome (middle), double metronome (bottom). Note the collapse and regeneration of one of the oscillator's amplitude in the metronome cases. The time scale on the horizontal axis refers to the number of integration steps. The frequency dependence of the stationary amplitude r is plotted in the right column for the three cases. In each case, squares and full circles denote antiphase and inphase motion obtained from the numerical simulations. The solid and dotted lines denote antiphase and inphase motion obtained from the mathematical analysis. Additionally in the two metronome cases, the inverted u-shape behavior of the stationary amplitudes is plotted which is obtained when the eigenfrequency ω of the fingers is constant.

Table II. Critical transition frequencies for self-paced (HKB) and paced (single and double metronome condition) movement. In the first row the experimentally observed increase of critical frequencies is stated. The second row refers to the analytic computation and the third row to the numerical simulations of the critical transition frequencies. In all conditions the eigenfrequency ω was varied as the metronome frequency Ω

HKB	Single	Double
$\omega_{c0} < \omega_{c1} < \omega_{c2}$		
$\sqrt{\frac{4\gamma\beta+\alpha A}{-3\alpha B}}$	$\left(\frac{-\epsilon_0^2}{4(3\alpha+\gamma)}\right)^{1/3}$	$\frac{-\epsilon_0}{2(3\alpha+\gamma)}$
1.2	1.6	2.4

On the rhs of Figure 4 the stationary amplitudes (antiphase: squares, inphase: full circles) obtained from numerical simulations are plotted over the frequency Ω for all three cases, together with the analytic results (antiphase: dotted line, inphase : solid line) obtained from (HKB: (47); single: (43), (44); double: (32), (33)). At high frequencies the antiphase state is terminated by the critical transition frequency, at low frequencies it becomes unstable and diverges. This lower bound is due to amplitude effects of the β-terms beyond our analytic considerations. The numerical results yield the existence of the stable antiphase state on the following plateaus: (HKB) $\omega = 0.85-1.18$, (single) $\omega = 1.15-1.5$, (double) $\omega = 0.75-2.9$. In Figure 4 the lower bounds of the plots of the analytically and numerically obtained antiphase states are determined by the numerically given instability points. The upper bounds of the plots of the analytically obtained antiphase states are given by the critical frequencies in Table II, the upper bounds of the numerically obtained antiphase states by the transition to the inphase state. The inphase state is stable for all conditions over the entire considered frequency range. The parameters used in the numerical simulations are given in Table I.

As originally suggested in (Haken *et al.*, 1985) we considered the eigenfrequency ω of the oscillators x_1, x_2 to be equal to the movement frequency for all conditions. This can be justified by a change in the linear stiffness of the oscillator, presumably caused by changes in length-tension characteristics of corresponding muscles (see e.g. (Feldman, 1980a; Feldman, 1980b) and (Beek *et al.*, 1995) for a description of the ω-approach applied to oscillators). However, note that such changes would be represented in changes of all the parameters A, B, γ and ω in (16).

If we drop the condition of the identity between eigenfrequency and movement frequency for the single and double metronome case and assume $\omega = \text{const}$, then the stationary solutions of ϕ_1, ϕ_2 will change in dependence of ω and Ω. In a first approximation (under conditions of parametric stabilization) the new stable stationary solutions of the phases ϕ_1, ϕ_2 in the single metronome case are

$$\phi_i = \frac{1}{2}\arccos\left(\frac{4\omega^2}{\epsilon_0^2}(\omega^2 - \Omega^2) - 1\right) \qquad \text{modulo } \pi \qquad i = 1, 2 \tag{48}$$

and in the double metronome case

$$\phi_i = \frac{1}{2}\arccos\left(\frac{\Omega^2 - 4\omega^2}{2\epsilon_0}\right) \qquad \text{modulo } \pi \qquad i = 1, 2 \tag{49}$$

Introducing these stationary solutions into the corresponding amplitude equations of r_1, r_2 yields an inverted u-shape behavior of the stationary amplitudes in dependence of ω, Ω. The inverted u-shape behavior originates in the finite width of an Arnold tongue (see Figure 2). We keep $\omega = 1.9$ and plot the value of the stationary amplitudes r_1, r_2 as circles on the rhs in Figure 4 in dependence of Ω for the single and in dependence of $\frac{1}{2}\Omega$ for the double metronome case. The stationary amplitudes show in both cases inverted u-shape approximately centered around ω.

In the single metronome case the instability region corresponding to $\omega = \frac{1}{2}\Omega$ is visible for frequencies higher than 3 and predicts that, when the eigenfrequency ω is sufficiently constant, a transition in the finger movements from single metronome to double metronome dynamics is to be observed. The double metronome dynamics, meaning the metronome frequency is twice the movement frequency, is the only possible subharmonic movement-metronome ratio (as can also be seen in Figure 2).

4.2. CRITICAL TRANSITION FREQUENCIES AND PARAMETER RANGES

A comparison of the critical movement frequencies ω_{c0} (self-paced, Equation (8)), ω_{c1} (single metronome, Equation (42)) and ω_{c2} (double metronome, Equation (34)), where the transition from antiphase to inphase occurs, allows a comparison of the stabilization effects due to the metronome. The exact critical frequencies will depend on the details of the multiplicative coupling in (10). For completeness, here we provide the results for the multiplicative coupling term ($c_1 = 1, d_1 = 0$) we discussed.

As observed experimentally (Fink *et al.*, 1998) the critical frequency increases from left to right in Table II, thus the stability of the antiphase pattern also increases from left to right. In the two conditions involving the metronome the same set of parameters has been used. The parameter γ describes linear dissipation (negative or positive) of energy and is different (see Table I) in the self-paced condition (HKB) than in the two metronome conditions. The metronome provides energy/information via the coupling term with ϵ_0. The presence of both energy sources in the model increases the oscillator amplitudes over a critical value such that the antiphase state in the single metronome condition is unstable. For this reason, we must assume that both energy sources are not present at the same time. When the metronome is turned off, the parameter γ changes to compensate for the lack of energy input. Another way to overcome this problem is to postulate some kind of 'internal metronome' serving as a pacemaker or central pattern generator for self-paced movement. When the external metronome is turned off, the internal metronome takes over. The prior solution implies that the task dependence is reflected in the parameters involved with the energy sources; the latter implies the possibility of the presence of phenomena in self-paced movements, e.g. anchoring phenomena, which were originally attributed only to coordination with external metronomes.

The critical frequencies in Table II were calculated based upon the assumption that the eigenfrequency ω varies with the movement frequency for all three conditions. Note that in the single metronome case the critical movement frequency ω_{c1} becomes

$$\frac{-\epsilon_0^2}{4\omega^2(3\alpha + \gamma)} \tag{50}$$

if the eigenfrequency ω stays approximately constant. The first row in Table II states the experimentally observed increase of the critical transition frequencies. The comparison of the analytic results (given in the second row of Table II) between the single and double metronome condition provides constraints on the numerical values of the parameters $\epsilon_0, \alpha, \omega$ (γ is neglected in the metronome conditions). Theoretically, a strong increase in coupling strength ϵ_0 would violate the empirical inequality $\omega_{c1} < \omega_{c2}$ and cause the single metronome condition to be more stable. We investigated the available parameter space for varying ϵ_0 and constant α. The eigenfrequency ω was either kept constant ($\omega = 1.3$) or varied as the metronome frequency Ω which provided similar results in both cases. For $\epsilon_0 < 2.4$ the antiphase state is not stable in the single metronome condition. $2.4 < \epsilon_0 < 3.1$ represents the parameter region for which our model of parametric stabilization reproduces inphase and antiphase coordination for both metronome conditions and a single parameter set as given in Table I. This parameter region satisfies the experimentally observed inequality $\omega_{c1} < \omega_{c2}$ and actually provides its upper limit in the case of constant eigenfrequency ω. For $\epsilon_0 > 3.1$ a subharmonic arises in the antiphase single metronome condition and destabilizes the antiphase state for $\epsilon_0 > 3.3$. For larger values of $\epsilon_0 \approx 4$, the subharmonics also show in the inphase state of the single metronome conditions.

4.3. VALIDITY AND LIMITATIONS OF THE APPROXIMATED AMPLITUDE DYNAMICS

We have employed a description of the transition behavior by means of an amplitude dynamics which is based on the approximations in (25),(26). However, when the amplitude r_i crosses the coordinate axis during the transition, a mathematical singularity occurs in the exact phase equations (22),(23) due to r_i in the denominator. At this point the phase ϕ_i is not locked anymore and the approximations (25),(26) are not valid. Here we want to test the goodness of our description in terms of amplitude dynamics for the double metronome case. The same arguments and results apply also to the single metronome case. We performed numerical simulations of the time evolution of the phases ϕ_i and amplitudes r_i of the exact system, now referred to as system I, given by (20),(21),(22),(23) and the approximated system, referred to as system II, given by (20),(21),(25),(26).

Shown in Figure 5 on the left, both systems were prepared with the same initial conditions and parameter values from Table I such that they perform the transition from antiphase to inphase. In the top row the time evolution of r_1 is plotted, for one generated by the exact system I and for the other generated by the approximated system II. The phase and amplitude evolution of systems I and II are denoted by a thin solid or bold dashed line, respectively. Both transients show a very good overlap exhibiting a slight increase of the amplitude r_1. The oscillator's phase ϕ_1, plotted in the row below, stays constant during the transition for both systems. In the third row the time evolution of the amplitude r_2 is plotted, and in the fourth

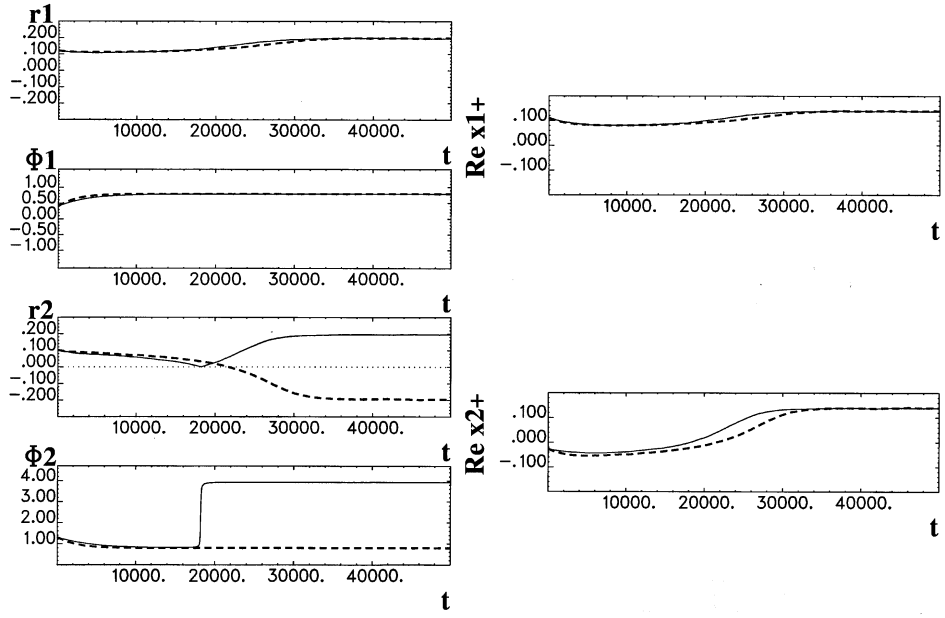

Figure 5. Phase and amplitude dynamics during the transition. The solid line denotes the time series generated by the exact system and the dashed line the time series generated by the approximated system. The time scale on the horizontal axis refers to the number of integration steps. Left column: The two top rows show the amplitude r_1 and phase ϕ_1 of oscillator 1 during the transition and then relaxing into a stationary state. The bottom two rows show the same time series for oscillator 2. The horizontal dotted line in the third row denotes the zero-axis which when approached by the exact solution of r_2 (solid line) causes an immediate transition by π of ϕ_2. The approximate solution of r_2 crosses instead the zero-axis and does not perform a transition of ϕ_2. Right column: The time series of the complex amplitudes x_{1+} (top) and x_{2+} (bottom) are reconstructed from their phase and amplitude values on the lhs. The real parts of these complex amplitudes are plotted over time and allow a comparison between exact solutions and approximations.

row its phase ϕ_2. The amplitude r_2 decreases for both systems to a critical value at which the phase ϕ_2 of the exact system performs a sudden transition by π which causes the immediate increase of the oscillator's amplitude r_2 in the vicinity $r_2 \approx 0$. The amplitude r_2 of system II, however, crosses the horizontal coordinate-axis (thin dotted line) and reaches a negative stationary amplitude state which is precisely the negative value displayed by system I. The phase ϕ_2 of system II remains constant throughout the entire transient process. We reconstruct the complex amplitude of the oscillators x_1 and x_2 from phase and amplitude of systems I and II using (19). Shown in Figure 5 on the right, the real part of x_{1+} is plotted in the top row and the real part of x_{2+} in the bottom row. The reconstruction of the oscillator amplitudes from the approximated system II is good for the transients, but in particular for the stationary states. The description in terms of an amplitude dynamics affords a simplified description of the transient dynamics, but still captures in an elegant way

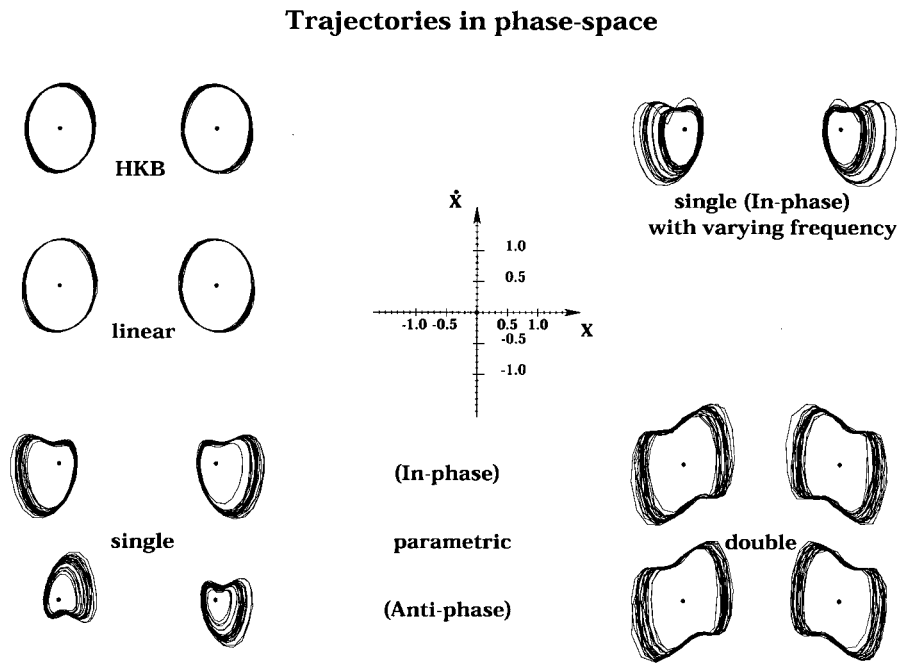

Figure 6. Numerically simulated phase plane trajectories of finger movements. The underlying x-$\dot{x}$-coordinate system of the left finger movement and its scales are plotted in the center. The right finger trajectories' x-axis is reversed. Left column: phase portraits of left and right finger movement generated under different stimulus conditions, namely self-paced (HKB, top row), linear driving (second row) and parametric driving (bottom row, single metronome condition). In the latter the inphase and antiphase conditions are distinguished. Right column: In the bottom row the phase portraits of left and right finger movement are plotted for the double metronome condition, also distinguishing inphase and antiphase coordination states. In the top right corner, the phase portraits of left and right finger movement are plotted for the single metronome condition in the inphase state under varying metronome frequency. Note that the anchoring points of flexion (compare to Figure 1) are fixed in phase space, even though the frequency and thus the amplitude varies.

both transition phenomena, namely the transition from antiphase to inphase and its accompanying amplitude changes.

4.4. TRAJECTORIES IN PHASE SPACE AND ANCHORING PHENOMENA

In Figure 6 we compare the left and right finger trajectories in the phase space ($x - \dot{x}$ – plane) for the self-paced conditions (HKB), linear driving as in (Schöner and Kelso, 1988a) and parametric excitation with single and double metronome. The underlying coordinate system for the left finger dynamics corresponding to the left trajectory of each condition is shown in the middle of Figure 6. In the coordinate system of the right finger trajectory the x-axis is reversed. The big dot in each trajectory corresponds to the origin of the coordinate system. All simulations

are performed for the parameters in Table I. The strength of the linear driving is $c_0\epsilon_0 = 1$. We also added Gaussian white noise $\xi(t)$ to the evolution equations (16), where

$$< \xi(t) >= 0 \qquad < \xi(t)\xi(\tau) >= Q^2\delta(t-\tau) \qquad Q = 0.01 \tag{51}$$

in order to enhance the anchoring phenomena. The triangular brackets denote time averages.

Figure 6 clearly shows that no anchoring phenomena are observed in the HKB model or in the linearly driven oscillators. Clear anchoring phenomena are only observed in the parametrically excited system for the single metronome case. Here the shape of the trajectories is asymmetric due to anchoring and reverses from antiphase to inphase as experimentally observed. The anchoring point remains spatially constant in the phase space under variation of the movement frequency ω, even though the amplitude changes. This can be seen in Figure 6 (top right) where the trajectories are shown for the single metronome condition (inphase) for the frequencies $\omega = \Omega = 1.3$ and $\omega = \Omega = 1.6$. The phenomenon of a spatially fixed reversal point under metronome impact is well-known in the literature (see e.g. (Byblow *et al.*, 1994)) and was also observed by (Fink *et al.*, 1998). In each trajectory of the single metronome case the anchoring point is shifted closer to the origin of the coordinate system than the other reversal point. This shift is quantified in Equation (36) and can be easily experimentally tested. In the double metronome case the shape of the trajectories is symmetric for antiphase and inphase. There is no anchoring point and both reversal points have the same distance from the center which is the origin of the underlying coordinate system, i.e. no horizontal shift is observed as in the single metronome case. As frequency increases the trajectory contracts centrally. This behavior is consistent with the experimental data.

5. Conclusions

In much previous research on coordination, a metronome has been used to implement frequency changes that alter the coordination dynamics. Yet, the metronome may also provide a source of specific environmental information on the dynamics. For instance, it may help in the coupling of action and perception, e.g., as a means to coincide the timing of an action; relatedly, specific information from the environment may stabilize or consolidate the action-perception cycle. For the paradigmatic case of bimanual coordination we studied the impact of a metronome on the coordination dynamics at both collective and component levels. Specifically, we established coupling terms, linear additive and multiplicative, describing the interaction between finger movements and the metronome and showed that multiplicative coupling is the better candidate for being used by the nervous system. The latter we termed parametric stabilization. Actually, our model of parametric stabilization must also be capable to describe the situation in (Kelso *et al.*, 1990) where a single finger movement is coordinated with an external metronome and

transition phenomena from antiphase to inphase are observed. Here it turns out that parametric stabilization creates the ability for bistability within the frame work of HKB modelling. This becomes obvious from inspection of the phase equation (63) where r_2 can be set to zero to reproduce the single limb-metronome coordination case. The only term which can cause bistability is the term stemming from the parametric drive. The destabilization of the antiphase requires a small contribution of the linear additive driving term in Equation (16) with $x_2(t), \dot{x}_2(t) = 0 \quad \forall\, t$, the parameter set in Table I and $c_0 = 0.07$. Since $c_0 \ll c_1$ as required in Section 3.3, the dynamics for bimanual coordination is not changed by this modification. Numerical simulations show that the transition phenomena observed in (Kelso *et al.*, 1990) can be reproduced by this model. Thus our extension of the HKB-coupling in Section 3 to situations in which a metronome is involved seems to hold also for more general situations of single limb and multilimb coordination.

Summarizing, our model of parametric stabilization preserves all the main characteristics of the HKB-model for bimanual coordination and hence also its consequent developments, e.g. the inclusion of stochastic fluctuations (Schöner *et al.*, 1986) and symmetry breaking (Kelso *et al.*, 1990): For example, at the collective level, coexistence of antiphase and inphase states; bistability below a critical movement frequency, monostability above; transition from antiphase to inphase at a critical frequency; phase shifts and drift; critical fluctuation enhancement, slowing down and switching times. And at the component level, limit cycle stability in the face of perturbations; frequency-amplitude changes; geometry of trajectories. By now treating the metronome as a specific source of environmental information on the dynamics, for a single set of parameters, our parametric stabilization model accomodates the following additional features: single and double metronome action-perception coupling; the increased stability of the double versus single metronome condition; the symmetric (double) versus asymmetric (single) geometry of the phase-plane trajectories, including trajectory thinning in the latter at the reversal points where the metronome occurs; shifts in phase space of the anchoring point between double and single metronome conditions as frequency increases. All these novel effects, observed experimentally, are quantified analytically. Important further predictions are the asymmetric transition from antiphase to inphase via break down of the amplitude of one oscillator in the case of parametric stabilization. This effect is distinct from the symmetric self-paced transition in the HKB model in which both oscillators preserve equal amplitudes. Also, transitions from single metronome coordination to double metronome coordination are expected for large metronome frequencies. Finally, the inverted u-shape frequency dependence of movement amplitude may also be understood in this context.

We hypothesize that the here presented interaction mechanisms with a metronome – conceptualized by the term parametric stabilization – will find wide use in modelling and understanding of coordination behavior where environmentally specified information is essential for maintaining a rhythmic pattern. More generally, we see via the concept of parametric stabilization how synchronizing an effector

with the environment – so-called anchoring – can lead to more global coordinative consequences, such as the stabilization of coordination under conditions in which it would normally change. Parametric stabilization thus affords biological systems an additional means of adapting to changes in the environment.

Appendix

A. Stationary solutions and linear stability analysis

Consider the system

$$\dot{r}_1 = ar_1 + br_2 - cr_1^3 \tag{52}$$

$$\dot{r}_2 = ar_2 + br_1 - cr_2^3 \tag{53}$$

which correponds to the systems (20),(21) in the double frequency case and (40),(41) in the single frequency case. The terms in β are neglected, since they change the amplitude dynamics only quantitatively, but not qualitatively within the considered parameter range. This is valid for the case of parametric stabilization and has been tested numerically. The phases ϕ_1, ϕ_2 are in their stable stationary states: $\phi_i = \pm\pi/4$ modulo π (double: +, single: –) for $i = 1, 2$. The coefficients are

$$a = \frac{\gamma+\alpha}{2} + \frac{\epsilon_0}{2\Omega}\sin 2\phi_1 \qquad b = -\frac{\alpha}{2}\cos\phi \qquad c = \frac{1}{2}(A + \frac{3}{4}B\Omega^2) \tag{54}$$

for the double frequency case and

$$\begin{aligned} a &= \frac{\gamma+\alpha}{2} - \frac{\epsilon_0^2}{8\Omega\omega^2}\sin 2\phi_1 \qquad b = -\frac{\alpha}{2}\cos\phi \\ c &= \frac{1}{2}(A(\frac{\epsilon_0^2}{2\omega^4}(\cos 2\phi_1 + 1) + 1) + 3B\Omega^2) \end{aligned} \tag{55}$$

for the single frequency case.

We set $\dot{r}_1 = \dot{r}_2 = 0$ to determine the stationary amplitude solutions. Then r_2 can be written as $r_2 = (cr_1^3 - ar_1)/b$ yielding the ninth-order polynomial

$$ab^2(cr_1^3 - ar_1) + b^4 r_1 - c(cr_1^3 - ar_1)^3 = 0 \tag{56}$$

The trivial solution $r_1 = r_2 = 0$ is a stationary solution. We take $r_1 \neq 0$, substitute $u = cr_1^2 - a$ and obtain the polynomial

$$u^4 + au^3 - ab^2u - b^4 = (u^2 - b^2)(u^2 + au + b^2) = 0 \tag{57}$$

from which we can determine the non-trivial stationary solutions

$$r_1^2 = \frac{a+b}{c} \qquad r_1 = r_2 \qquad \rightarrow \text{Inphase} \tag{58}$$

$$r_1^2 = \frac{a-b}{c} \qquad r_1 = -r_2 \qquad \rightarrow \text{Antiphase} \tag{59}$$

$$r_1^2 = \frac{a}{2c}(1 \pm \sqrt{a^2 - 4b^2}) \qquad r_2^2 = \frac{a}{2c}(1 \mp \sqrt{a^2 - 4b^2}) \tag{60}$$

We linearize the system (52),(53) around its stationary solutions and determine the eigenvalues λ from the characteristic polynomial:

$$\lambda = \frac{1}{2}(2a - 3c(r_1^2 + r_2^2) \pm \sqrt{9c^2(r_1^2 - r_2^2)^2 + 4b^2}) \tag{61}$$

The inphase state (58) is always stable, the trivial zero-state and (60) are unstable for both metronome conditions. The antiphase state is stable below a critical frequency which is given by

$$\lambda = -2a + 4b = 0 \qquad \longrightarrow \qquad \Omega_c = \begin{cases} \frac{-\epsilon_0^2}{4\omega^2(3\alpha+\gamma)} & \text{single} \\ \frac{-\epsilon_0}{2(3\alpha+\gamma)} & \text{double} \end{cases} \tag{62}$$

For movement frequencies higher than Ω_c the antiphase state becomes unstable.

B. Full oscillator equations: Single frequency case

The full phase equations are

$$\begin{aligned} \dot{\phi}_1 \;=\; & \tfrac{\omega^2-\Omega^2}{2\Omega} + \tfrac{1}{2}(\alpha + \beta(r_1^2 + r_2^2 - 2r_1 r_2 \cos\phi \\ & + \tfrac{\epsilon_0^2}{\omega^4}(r_1\cos\phi_1 - r_2\cos\phi_2)^2))\tfrac{r_2}{r_1}\sin\phi \\ & - \tfrac{1}{2}\beta r_2^2 \sin 2\phi - \tfrac{\epsilon_0^2}{8\Omega\omega^2}(\cos 2\phi_1 + 1) - \tfrac{c_0\epsilon_0}{2\Omega r_1}\cos\phi_1 \end{aligned} \tag{63}$$

$$\begin{aligned} \dot{\phi}_2 \;=\; & \tfrac{\omega^2-\Omega^2}{2\Omega} + \tfrac{1}{2}(\alpha + \beta(r_1^2 + r_2^2 - 2r_1 r_2 \cos\phi \\ & + \tfrac{\epsilon_0^2}{\omega^4}(r_1\cos\phi_1 - r_2\cos\phi_2)^2))\tfrac{r_1}{r_2}\sin\phi \\ & + \tfrac{1}{2}\beta r_1^2 \sin 2\phi - \tfrac{\epsilon_0^2}{8\Omega\omega^2}(\cos 2\phi_2 + 1) - \tfrac{c_0\epsilon_0}{2\Omega r_2}\cos\phi_2 \end{aligned} \tag{64}$$

The full amplitude equations are

$$\begin{aligned} \dot{r}_1 \;=\; & \tfrac{\gamma+\alpha}{2}\, r_1 - \tfrac{\alpha}{2}\, r_2 \,\cos\phi - \tfrac{1}{2}(A(\tfrac{\epsilon_0^2}{2\omega^4}(\cos 2\phi_1 + 1) + 1) + 3B\Omega^2)\, r_1^3 \\ & + \tfrac{\beta}{2}(\tfrac{\epsilon_0^2}{\omega^4}(r_1\cos\phi_1 - r_2\cos\phi_2)^2 + r_1^2 + r_2^2 - 2r_1 r_2\cos\phi)(r_1 \\ & - r_2\cos\phi) - \tfrac{\epsilon_0^2}{8\Omega\omega^2}\sin 2\phi_1\, r_1 - \tfrac{c_0\epsilon_0}{2\Omega}\sin\phi_1 \end{aligned} \tag{65}$$

$$\dot{r}_2 = \frac{\gamma+\alpha}{2} r_2 - \frac{\alpha}{2} r_1 \cos\phi - \frac{1}{2}(A(\frac{\epsilon_0^2}{2\omega^4}(\cos 2\phi_1 + 1) + 1) + 3B\Omega^2)\ r_2^3$$
$$+\frac{\beta}{2}(\frac{\epsilon_0^2}{\omega^4}(r_1\cos\phi_1 - r_2\cos\phi_2)^2 + r_1^2 + r_2^2 - 2r_1r_2\cos\phi)(r_1 \qquad (66)$$
$$-r_2\cos\phi) - \frac{\epsilon_0^2}{8\Omega\omega^2}\sin 2\phi_2\ r_2 - \frac{c_0\epsilon_0}{2\Omega}\sin\phi_2$$

Acknowledgement

This research was supported by NIMH grants MH 42900 and KO5 MH 01386 and The Human Frontiers Science Program.

References

Amazeen, P.G., Schmidt, R.C. and Turvey, M.T. (1995) Frequency detuning of the phase entrainment dynamics of visually coupled rhythmic movements, *Biol. Cybern.* **72**, 511–518.

Beek, P.J., Schmidt, R.C., Morris, A.W., Sim, M.Y. and Turvey, M.T. (1995) Linear and nonlinear stiffness and friction in biological rhythmic movements, *Biol. Cybern.* **73**, 499–507.

Byblow, W.D., Carson, R.G. and Goodman, D. (1994) Expressions of asymmetries and anchoring in bimanual coordination, *Human Movement Science* **13**, 3–28.

Carson, R.G. (1995) The dynamics of isometric bimanual coordination, *Exp. Brain Res.* **105**, 465–476.

Carson, R.G., Byblow, W.D. and Goodman, D. (1994) The dynamical substructure of bimanual coordination. In: S.P. Swinnen, H. Heuer, J. Massion and P. Caesar (eds.), *Interlimb Coordination: Neural, Dynamical, and Cognitive Constraints*, Academic Press New York, pp. 278–300.

DeGuzman, G.C. and Kelso, J.A.S. (1991) Multifrequency behavioral patterns and the phase attractive circle map, *Biol. Cybern.* **64**, 485–495.

Elias, S. and Grossberg, S. (1975) Pattern formation, contrast control, and oscillations in the short term memory of shunting on-center off-surround networks, *Biol. Cybern.* **20**, 69–98.

Feldman, A.G. (1980a) Superposition of motor programs. I. Rhythmic forearm movements in man, *Neuroscience* **5**, 81–90.

Feldman, A.G. (1980b) Superposition of motor programs. II. Rapid flexion of forearm in man, *Neuroscience* **5**, 91–95.

Fink, P.W., Kelso, J.A.S., Jirsa, V.K. and Foo, P. (1998) Informational stabilization of bimanual finger coordination, *Journal of Sport and Exercise Psychology* **20**, S33.

Fink, P.W., Foo, P., Jirsa, V.K. and Kelso, J.A.S. (1999) Local and global stabilization of coordination by sensory information, *Exp. Brain Res.*, in press.

Grossberg, S., Pribe, C. and Cohen, M.A. (1997) Neural control of interlimb oscillations. I. Human bimanual coordination, *Biol. Cybern.* **77**, 131–140.

Guckenheimer, J. and Holmes, P. (1983) *Nonlinear oscillations, dynamical systems, and bifurcations of vector fields*, Springer, New York.

Haken, H. (1983) *Synergetics. An Introduction, 3rd ed.*, Springer, Berlin.

Haken, H. (1987) *Advanced Synergetics. 2nd ed.*, Springer, Berlin.

Haken, H. (1996) *Principles of brain functioning*, Springer, Berlin.

Haken, H., Kelso, J.A.S. and Bunz, H. (1985) A Theoretical Model of Phase transitions in Human Hand Movements, *Biol. Cybern.* **51**, 347–356.

Haken, H., Peper, C.E., Beek, P.J. and Daffertshofer, A. (1996) A model for phase transitions in human hand movements during multifrequency tapping, *Physica D* **90**, 179–196.

Hodgkin, A.L. and Huxley, A.F. (1952) A quantitative description of membrane current and its application to conduction and excitation in nerve, *J. Physiol.* **117**, 500–544.

Jirsa, V.K. and Haken, H. (1996) Field theory of electromagnetic brain activity, *Phys. Rev. Let.* **77**, 960–963.

Jirsa, V.K. and Haken, H. (1997) A derivation of a macroscopic field theory of the brain from the quasi-microscopic neural dynamics, *Physica D* **99**, 503–526.

Jirsa, V.K., Fuchs, A. and Kelso, J.A.S. (1998) Connecting cortical and behavioral dynamics: bimanual coordination, *Neural Computation* **10**, 2019–2045.

Kay, P.A., Kelso, J.A.S., Saltzmann, E.L. and Schöner, G. (1987) Space-time behavior of single and bimanual rhythmical movements: data and limit cycle model, *J. Exp. Psych.* **13**, 178–192.

Kelso, J.A.S. (1981) On the oscillatory basis of movement, *Bull. Psychon. Soc.* **18**, 63.

Kelso, J.A.S. (1984) Phase transitions and critical behavior in human bimanual coordination, *Am. J. Physiol.* **15**, R1000–R1004.

Kelso, J.A.S. (1995) *Dynamic Patterns. The Self-Organization of Brain and Behavior*, The MIT Press, Cambridge, Massachusetts.

Kelso, J.A.S., Scholz, J.P. and Schöner, G. (1986) Nonequilibrium phase transitions in coordinated biological motion: critical fluctuations, *Phys. Let. A* **118:**, 279–284.

Kelso, J.A.S. and DeGuzman, G.C. (1988) Order in time: How cooperation between the hands informs the design of the brain. In: H. Haken (ed.), *Neural and Synergetic Computers*, Springer Berlin, pp. 180–196.

Kelso, J.A.S., DelColle, J.D. and Schöner, G. (1990) Action-perception as a pattern formation process. In: M. Jeannerod (ed.), *Attention and performance XIII*, Erlbaum, Hillsdale, NJ, pp. 136–169.

Kelso, J.A.S., DeGuzman, G.C. and Holroyd, T. (1991) Synergetic dynamics of biological coordination with special reference to phase attraction and intermittency. In: H. Haken and H.P. Köpchen (eds.), *Rhythms in Physiological Systems, Springer Series in Synergetics* **55**, Springer Berlin, pp. 195–213.

Kelso, J.A.S. and Jeka, J.J. (1992) Symmetry breaking dynamics of human multilimb coordination, *J. Exp. Psych.: Human Perception and Performance* **18**, 645–688.

Kelso, J.A.S., Fuchs, A., Holroyd, T., Cheyne, D. and Weinberg, H. (1994) Bifurcations in human brain and behavior, *Soc. f. Neuroscience* **20**, 444.

Nagashino, H. and Kelso, J.A.S. (1992) Phase transitions in oscillatory neural networks, *Science of Artificial Neural Networks, SPIE* **1710**, 278–297.

Pribe, C., Grossberg, S. and Cohen, M.A. (1997) Neural control of interlimb oscillations. II. Biped and quadruped gaits and bifurcations, *Biol. Cybern.* **77**, 141–152.

Schmidt, R.C., Shaw, B.K. and Turvey, M.T. (1993) Coupling dynamics in interlimb coordination, *J. Exp. Psych.: Human Perception and Performance* **19**, 397–415.

Scholz, J.P., Kelso, J.A.S. and Schöner, G. (1987) Nonequilibrium phase transitions in coordinated biological motion: critical slowing down and switching time, *Phys. Let. A* **123**, 390–394.

Schöner, G., Haken, H. and Kelso, J.A.S. (1986) A stochastic theory of phase transitions in human hand movement, *Biol. Cybern.* **53**, 247–257.

Schöner, G. and Kelso, J.A.S. (1988a) A Synergetic Theory of Environmentally-Specified And Learned Patterns of Movement Coordination: I. Relative Phase Dynamics, *Biol. Cybern.* **58**, 71–80.

Schöner, G. and Kelso, J.A.S. (1988b) A Synergetic Theory of Environmentally-Specified And Learned Patterns of Movement Coordination: II. Component Oscillator Dynamics, *Biol. Cybern.* **58**, 81–89.

Treffner, P. and Turvey, M.T. (1996) Symmetry, broken symmetry, and handedness in bimanual coordination dynamics, *Exp. Brain Res.* **107**, 463–478.

Tuller B. and Kelso, J.A.S. (1989) Environmentally-specified patterns of movement coordination in normal and split-brain subjects, *Exp. Brain Res.* **75**, 306–316.

Zanone, P.G. and Kelso, J.A.S. (1992) Evolution of behavioral attractors with learning: nonequilibrium phase transitions, *J. Exp. Psych.: Human Perception and Performance* **18**, 403–421.